Inorganic Chemistry

Article

pubs.acs.org/IC

Synthesis and Structural Investigation of a Unique Columnar Phase in the $Bi_2O_3-TeO_2-V_2O_5$ System

Vaishali Thakral, Neha Bhardwaj, and S. Uma*

Materials Chemistry Group, Department of Chemistry, University of Delhi, Delhi—110007, India

Supporting Information

ABSTRACT: A new columnar phase $Bi_{11.65}Te_{1.35}V_5O_{34-\delta}$ ($\delta \sim 1.3$) containing VO_4 tetrahedra has been identified for the first time in the $Bi_2O_3-TeO_2-V_2O_5$ system. The phase formation and the extent of substitution of Te^{4+} for Bi^{3+} ions in order to stabilize V^{5+} in this composition have been confirmed by the single crystal analysis, combined with the powder X-ray diffraction of the solid state synthesized bulk crystalline samples. The oxide crystallizes in a monoclinic crystal system, space group $P2/c$, with unit cell parameters $a = 11.4616(7)$ Å, $b = 5.7131(3)$ Å, $c = 23.5090(18)$ Å, $\beta = 101.071°$ (6) ($Z = 2$). The structure retains the basic features of the columnar oxides with the presence of $[Bi_{10.65}Te_{1.35}O_{14}]_n^{9.35n+}$ columns along the (010) direction, surrounded by (VO_4) tetrahedra placed in the planes parallel to (100) and (001), with an isolated bismuth atom in between the columns. The composition with a limited Te^{4+} substitution, $Bi_{11.65}Te_{1.35}V_5O_{34-\delta}$ ($\delta \sim 1.3$), exists with a surprisingly high oxygen deficiency as compared to the stoichiometrically known columnar oxides such as $Bi_{13}Mo_4VO_{34}$, $Bi_{12}Te_1Mo_3V_2O_{34}$, and $Bi_{11}Te_2Mo_2V_3O_{34}$. The structure of this interesting member of the columnar family of oxides based on the single crystal X-ray diffraction and the Raman spectroscopic studies indicates the possibility of the distribution of the oxygen vacancies among the VO_4 tetrahedral units. Further confirmation for the formation of vanadium stabilized columnar structures has been provided by the successful preparation of $Bi_{11.65}Te_{1.35}V_4CrO_{34-\delta}$ ($\delta \sim 0.83$) and $Bi_{11.65}Te_{1.35}V_4WO_{34-\delta}$ ($\delta \sim 0.83$) phases. Preliminary investigation of the photocatalytic efficiencies of the oxides $Bi_{11.65}Te_{1.35}V_5O_{34-\delta}$, $Bi_{11.65}Te_{1.35}V_4CrO_{34-\delta}$, and $Bi_{11.65}Te_{1.35}V_4WO_{34-\delta}$ revealed moderate photocatalytic activities for the decomposition of the dyes such as Rhodamine B under UV—vis light irradiation.

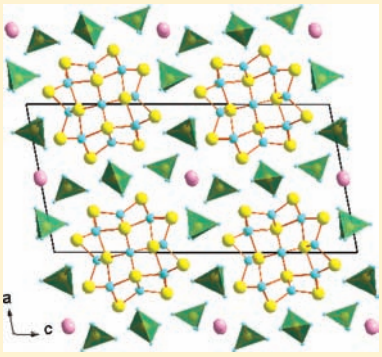

1. INTRODUCTION

The origin for the intensive investigation of the solid state chemistry of the oxides and mixed metal oxides of Bi(III) can be traced to the stereochemical nature of the lone pair. The significance of the structural diversity exhibited by the Bi(III) containing oxides is realized by their applications ranging from ferroelectricity,[1] selective oxidation catalysis,[2] ionic conductivity,[3] and photocatalysis.[4] δ-Bi_2O_3 with a fluorite structure, stabilized at high temperature, is a very well-known ionic conductor (1 S cm^{-1} at 750 °C).[5] Various metal ion substitutions (La^{3+}, Nd^{3+}, Eu^{3+}, Er^{3+}, Gd^{3+}, Y^{3+}, etc.) have been investigated for the stabilization of δ-Bi_2O_3 structure and to improve their ionic conductivities.[5] Consistently, several examples of bismuth based oxides are being investigated in order to understand the structure—property relation along with their associated applications. $Bi_2Mo_3O_{12}$, $Bi_2Mo_2O_9$, and γ-Bi_2MoO_6 are some of the well-known bismuth molybdates that are industrially important catalysts for the selective oxidation and ammoxidation.[6] In this context, the phase diagram and the different members belonging to the $Bi_2O_3-MoO_3$ phase diagram have been studied systematically by several groups.[7,8] The discoveries of $Bi_4V_2O_{11}$ and the entire BIMEVOX family ($Bi_4V_{2-x}M_xO_{11-\delta}$; M = metal ions) of oxides are the stand alone examples of oxides with an oxygen vacancy ordered structures causing a huge impact on the properties as shown by the considerably high ionic conductivity (e.g., $\sim 10^{-2}$ S cm^{-1} at 600 °C for γ-$Bi_4V_2O_{11}$).[9] A variety of novel and original structures have also resulted from the appropriate combination of Bi^{3+}/M^{2+} ions with P, V, As in the form of $((P/V/As)O_4)$ tetrahedra. Many of these bismuth oxy-phosphates, oxy-vanadates, and oxy-arsenates such as $BiMXO_5$ (M = Ni, Co, Mn, Pb, Cd; X = V/P/As)[10] and BiM_2XO_6 (M = Cu, Zn, Pb, Mn, Cd, Mg, Ca; X = V/P/As)[11,12] have been structurally identified and characterized to follow the lone pair stereoactivity coupled with the idea of discovering novel ferroelectric and nonlinear optical materials.

Our motivation to explore the ternary system of $Bi_2O_3-TeO_2-V_2O_5$ was manifold. A foremost aspiration was the structural modifications that can be arrived at by the inclusion of another lone pair cation (Te^{4+}) along with the Bi^{3+} cation. Also, out of this exploration, we envisaged new oxide ion conductors and/or visible light based photocatalysts. Although the aforementioned properties are not correlated, sufficient existence of Bi(III) containing mixed metal oxides along with a transition element (e.g., δ-Bi_2O_3, $Bi_4V_2O_{11}$,[3,9] Bi_2MoO_6,[13] etc.) can justify the expectation of materials with reasonable ionic conductivity. Similarly, photocatalytic activity depends ideally

Received: August 6, 2011
Published: January 17, 2012

   dx.doi.org/10.1021/ic2017159 | *Inorg. Chem.* 2012, 51, 1462–1470

on the electronic structure and the appropriate band gaps of the solids. Among other factors in particular, Bi(III) oxides are expected to contribute their 6s band to the valence band formation of the solid along with the O 2p band and make them suitable for visible light absorption.[4,14] Visible light photocatalytic activity for the water splitting as well as for the environmental remediation, as shown by the decomposition of harmful organics, has been reported for oxides such as $Bi_2PbNb_2O_9$,[15] $CaBi_2O_4$,[16] $BiVO_4$,[4] and $Bi_4V_2O_{11-\delta}$ and BIMEVOX (ME = Al, Ga).[17]

During a systematic investigation of Te^{4+} incorporation in the Bi−V−O system, a melt having Bi_2O_3:TeO_2:V_2O_5 in the ratio 1:1:1, on cooling resulted surprisingly in the formation of a large amount of crystals with a bismuth rich composition. Subsequent structure analysis by the single crystal X-ray diffraction confirmed the formation of $(BiTe)_{13}V_5O_{34-\delta}$ with a columnar $[(Bi/Te)_{12}O_{14}]$ rose structure. The columnar rose structure consisting entirely of vanadium oxygen tetrahedra, without the presence of molybdenum ions, has been realized for the first time. The rose type columnar structure has been a common feature observed in the crystal structures[18−22] of $Bi_{26}Mo_{10}O_{69}$, $Bi_{26}Mo_6V_4O_{67}$, and $Bi_{13}Mo_4VO_{34}$. $Bi_{26}Mo_{10}O_{69}$ is a pure oxide ion conductor with an ionic conductivity, 1 mS/cm at 500 °C, and low activation energy of 0.47 eV.[21] Compositions with columnar structure in the Bi−Mo−O ternary system were initially reported with a solubility range $2.57 \leq Bi/Mo \leq 2.77$. Later, the existence of the extended solubility range ($2.53 \leq Bi/Mo \leq 3.50$) of the solid solution has been proposed.[22] The basic structural feature is made up of MoO_4^{2-} tetrahedra surrounding the $[Bi_{12}O_{14}]_\infty$ columns along with a noncolumnar Bi atom in between the two tetrahedra.[18−20] $Bi_{26}Mo_{10}O_{69}$ crystallizes in the monoclinic symmetry (space group, $P2/c$) with cell parameters a = 11.7456(3) Å, b = 5.7988(1) Å, c = 24.47922(5) Å, and β = 102.903(1)°,[19] and $Bi_{13}Mo_4VO_{34}$ also crystallizes in the monoclinic symmetry (space group, $P2/c$) with cell parameters a = 11.652(7) Å, b = 5.7923(8) Å, c = 24.420(9) Å, and β = 101.38°.[20] Numerous substitutions have been carried out in order to isolate the structural variants and to understand the mechanistic pathway for the ionic conductivity. Substitution of ions such as Ca, Sr, Ba, and Pb in place of the noncolumnar bismuth are known in $[Bi_{12}O_{14}]_2[Bi_{2-x}Me_xMo_{10}O_{41-0.5x}]$ (Me = Pb; x = 0, 0.25, 0.50, 1.00, 1.25, 1.50, 2.00 and Me = Ba, Sr, Ca; x = 0.50, 1.00, 1.50, 2.00) compositions.[23,24] Furthermore, the noncolumnar bismuth can be replaced by the rare earth ions resulting in a series of columnar oxides, $Ln_{2/3}\square_{1/3}[Bi_{12}O_{14}](MoO_4)_5$ (□ = vacancy; Ln = La, Nd, Gd, Ho, and Yb) with enhanced ionic conductivity.[25] Substitution at the columnar bismuth is relatively limited and has been known to tolerate only the substitution of Te^{4+} ions. Charge compensation is thus required in this case and has been provided by the substitution of V^{5+} for Mo^{6+} in the synthesis of $Bi(Bi_{12-x}Te_xO_{14})Mo_{4-x}V_{1+x}O_{20}$ ($0 \leq x \leq 2.0$) solid solution members.[26] Substitutions at the molybdenum site in small amounts have also yielded oxides such as $Bi_{26}Mo_{10-x}P_xO_{69-0.5x}$ ($0 \leq x \leq 1.6$),[24] $Bi_{26}Mo_{10-x}W_xO_{69}$ ($0 \leq x \leq 2$),[24] $Bi[Bi_{12}O_{14}][(Mo,M)O_4]_5$ (M = Li, Mg, Al, Si, Ge, and V),[27] and $Bi_{26}Mo_9GeO_{68}$.[28] These studies based on intentional metal ion substitutions, apart from the idea of locating the isostructural members belonging to the family of oxides having the columnar structure, were also useful to discover oxides with better ionic conductivity.[27−29] Oxides such as $A_xBi_{26-x}Mo_{10}O_{68+0.5y}$ (A = Ba, y = 0; A = Bi, La, y = 2) have also been evaluated as potential photocatalytic materials for the decomposition of phenols and substituted phenols under UV light irradiation.[30]

Recently, $Bi_6Mo_2O_{15}$[31] with a structure resembling closer to $Bi_6Cr_2O_{15}$[32] has also been characterized from the powder X-ray diffraction. In these examples, the columnar rose type structure has been found to exist even with a higher Bi/Cr or Bi/Mo ratio (3.0:1) as compared to the Bi/Mo ratio (2.6:1) observed in the parent structure of $Bi_{26}Mo_{10}O_{69}$. As a consequence, each column in the former structure is surrounded only by eight (CrO_4) tetrahedra, while it is surrounded by 10 (MoO_4) tetrahedra in the latter. There are also two isolated noncolumnar bismuth atoms in the $Bi_6Cr_2O_{15}$ structure. In the current work, unprecedented, the columnar rose structure is stabilized for the composition $Bi_{11.65}Te_{1.35}V_5O_{34-\delta}$ ($\delta \sim 1.3$), as confirmed by the single crystal X-ray diffraction studies. Of course, the formation of the columnar structure with V^{5+} alone resembling closely $Bi_{26}Mo_{10}O_{69}$ or $Bi_{13}Mo_4VO_{34}$ could only be possible with an oxygen ion deficiency. However, the decrease in the positive charge, caused by the presence of V^{5+} ions instead of Mo^{6+} ions, to some extent is compensated by the presence of a small amount of Te^{4+} ions replacing the Bi^{3+} ions. The amount of Te^{4+} substituted for Bi^{3+} ions in order to stabilize V^{5+} in the composition $Bi_{11.65}Te_{1.35}V_5O_{34-\delta}$ has been established by the powder X-ray diffraction of the bulk crystalline samples synthesized by the solid state reactions. Independently, we synthesized the compositions $Bi_{11.65}Te_{1.35}V_4CrO_{34-\delta}$ ($\delta \sim 0.83$) and $Bi_{11.65}Te_{1.35}V_4WO_{34-\delta}$ ($\delta \sim 0.83$) and characterized their powder X-ray diffraction patterns. This work reports the synthesis, along with the single crystal and powder X-ray characterization and the photocatalytic evaluation of these new members of the columnar family of bismuth oxides.

2. EXPERIMENTAL SECTION

2.1. Synthesis. Initial phase identification was carried out from the single crystals obtained by melting and cooling of a mixture containing Bi_2O_3 (Aldrich, 99.9%), TeO_2 (Aldrich, 99.9%), and V_2O_5 (Aldrich, 99.8%) in the ratio 1:1:1 in a platinum crucible. The reactants were rapidly (300 °C/h) heated to 900 °C for 10 min, cooled to 700 °C at 2 °C/h, and then allowed to cool naturally in the furnace to room temperature. A mixture of light yellow, dark yellow, and transparent crystals thus obtained were studied by single crystal X-ray diffraction technique. Subsequently, several polycrystalline samples were attempted by mixing appropriate amounts of the reactants thoroughly in an agate pestle and mortar, and the ground samples were subjected to a heat treatment in platinum crucibles. A variety of heat treatments were examined, following the results derived from the powder X-ray diffraction studies, and have been discussed in detail in the Results and Discussion.

2.2. Characterization. Single crystal X-ray diffraction data was recorded on an Oxford Xcalibur MOVA diffractometer with a four-circle κ goniometer employing a graphite-monochromatized Mo Kα (λ = 0.710 73 Å) radiation at 180 K. The diffraction intensities were corrected for Lorentz and polarization effects. The data were reduced using CrysAlisRED (special programs available with the diffractometer), the shape and size of the crystal were determined with the video microscope attached to the diffractometer, and an analytical absorption correction (after Clark and Reid) from the crystal shape was applied. The structure was solved by direct methods and refined using SHELXS97.[33] The packing diagrams were generated by DIAMOND, version 3.[34] The compositions of the single crystals were also estimated using the field emission scanning electron microscope (FESEM, FEI Quanta 200F) with an EDAX attachment.

The powder X-ray diffraction patterns were collected using high resolution D8 Discover Bruker diffractometer, equipped with point detector (scintillation counter), employing Cu Kα radiation (λ =

dx.doi.org/10.1021/ic2017159 | Inorg. Chem. 2012, 51, 1462−1470

1.5418 Å) obtained through a göbel mirror with a scan rate of 1.0 s/step and step size 0.02° at 298 K. Using this data, Le Bail fit[35] was carried out by TOPAS 3 software,[36] wherein the background was estimated by a Chebychev polynomial function with 6 coefficients, and the peak shape was described by a pseudo-Voigt function. The zero error, shape parameters, lattice parameters, and the profile coefficients were refined to obtain a suitable fit. UV−vis diffuse reflectance data were collected over the spectral range 200−1000 nm using Perkin-Elmer Lambda 35 scanning double beam spectrometer equipped with a 50 mm integrating sphere. $BaSO_4$ was used as a reference. The data were transformed into absorbance with the Kubelka−Munk function for the estimation of the band gap. Raman spectra of the powder samples were collected using a Renishaw spectrophotometer equipped with a microscope and employing a laser wavelength of 514 nm.

2.3. Photocatalytic Experiments. The photochemical reactor used in the present study consisted of a quartz tube of dimensions, 2.5 cm i.d., 3.5 cm o.d., and 14 cm length. A medium pressure mercury vapor (MPML) lamp of 125 W (Phillips, India) was placed inside the reactor after carefully removing the outer shell. The light source assembly was placed inside a Pyrex glass container filled with the appropriate dye solution. Circulation of water was carried out to avoid heating during the reaction. A typical experiment of degradation was carried out as follows: 0.5 g of the catalyst was added to 150 mL of aqueous solution of Rhodamine B (Rh B) with an initial concentration of 5×10^{-6} mol/L for UV and visible irradiation experiments. Prior to the irradiation, the suspension of the catalyst and dye solution was stirred in dark for 30−60 min, so as to reach the equilibrium adsorption. Aliquots (5 mL) were pipetted out periodically from the reaction mixture. The solutions were centrifuged, and the concentrations of the solutions were determined by measuring the maximum absorbance (λ_{max} = 552 nm).

3. RESULTS AND DISCUSSION

Light yellow single crystals with an anticipated stoichiometry belonging to the ternary Bi_2O_3:TeO_2:V_2O_5 system was first observed, when the homogenized mixture of the respective oxides in the ratio 1:1:1 was melted around 900 °C and slow cooled. These light yellow crystals were clearly distinguishable from the other reaction products such as the bright yellow $BiVO_4$ and the white transparent Bi_2TeO_5 crystals. Subsequently, the EDAX analysis of the light yellow crystals confirmed the crystals to be consisting of Bi, Te, and V. The results further confirmed that the amount of vanadium with respect to bismuth and tellurium remained constant, while the amount of bismuth and tellurium varied and the ratio arriving out of the EDAX experiments seemed to suggest a Bi:Te:V ratio to be 2.6:0.47:1 (Figure S1). Preliminary experiments of these crystals in the single crystal X-ray diffractometer were carried out and were frequently indexed in a monoclinic crystal system with the lattice parameters $a \approx 11.45$ Å, $b \approx 5.72$ Å, $c \approx 11.77$ Å, and $\beta \approx 101.21°$. Occasionally, a doubling along the c direction was observed with the monoclinic cell parameters $a \approx 11.46$ Å, $b \approx 5.71$ Å, $c \approx 23.51$ Å, $\beta \approx 101.07°$. An immediate comparison of the crystal symmetry and lattice parameters indicated the structural resemblance, respectively, with that of $Bi_{12}TeMo_3V_2O_{34}$ and $Bi_{11}Te_2Mo_2V_3O_{34}$, the x = 1 and x = 2 solid solution members of the series Bi-$(Bi_{12-x}Te_xO_{14})Mo_{4-x}V_{1+x}O_{20}$.[26] The differences between the structures of these x = 1 and x = 2 correspond to the differences between that of a noncentrosymmetric (x = 1, space group $P2$, No. 3) and centrosymmetric (x = 2, space group $P2/c$, No. 13) structures. The absence of the center of inversion (at $^1/_2$, $^1/_2$, 0) from the latter results in an acentric structure with a decrease in the c lattice parameter by half in the former.

The unexpected stabilization of the columnar phase in the Bi_2O_3−TeO_2−V_2O_5 system prompted us to do the phase verification through the synthesis of polycrystalline samples. The preparation of the phase pure bulk powder samples was also very much essential to determine the extent of incorporation of Te^{4+} ions for the stabilization of a columnar rose containing oxide. On the basis of the stoichiometry of a parent oxide such as $Bi_{13}Mo_4VO_{34}$, a nominal composition of $Bi_9Te_4V_5O_{34}$ would be justified, ideally for the complete replacement of V^{5+} for Mo^{6+} ions. A stoichiometric mixture of the reactants (Bi_2O_3, TeO_2, V_2O_5) with a target composition of $Bi_9Te_4V_5O_{34}$ was heated in the platinum crucibles in steps at the various temperatures of 500, 600, 650, 700, and 750 °C for 12 h. The powder samples initially were annealed after each thermal treatment, and the powder X-ray diffraction patterns invariably revealed the presence of products, such as Bi_2TeO_5 and $BiVO_4$ (Figure S2). Modifications of the thermal treatments were then examined, wherein the homogenized reactants in the platinum crucibles were introduced into a preheated (700 °C) furnace, held for 12 h, followed by a rapid quenching in air. This cycle of fast heating and quenching was repeated again at a temperature of 750 °C. The corresponding powder X-ray diffraction pattern showed the formation of a columnar type phase along with $BiVO_4$ impurity (Figure 1).

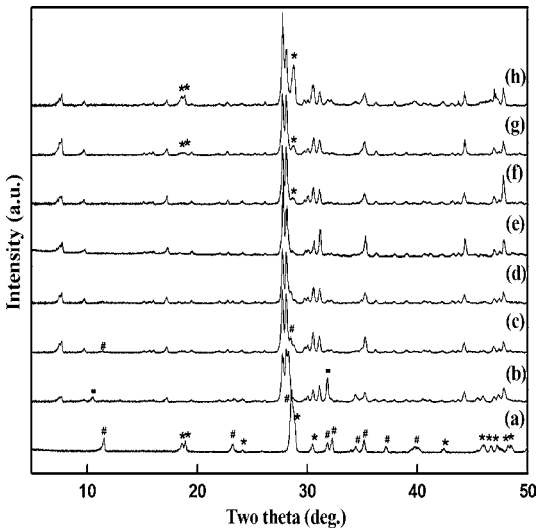

Figure 1. Powder X-ray diffraction patterns of the polycrystalline samples with varying amounts of Te^{4+}, $Bi_{13-x}Te_xV_5O_{34-\delta}$ (a) x = 0, (b) x = 1, (c) x = 1.25, (d) x = 1.35, (e) x = 1.40, (f) x = 1.5, (g) x = 2.0, and (h) x = 4 (#, *, and ■ represent γ-$Bi_4V_2O_{11}$/substituted BIMEVOX (ME = Te), $BiVO_4$, and unidentified impurities).

Subsequently, we attempted to synthesize the polycrystalline samples with varying amounts of Te^{4+}, $Bi_{13-x}Te_xV_5O_{34-\delta}$ (x = 0, 1, 1.25, 1.35, 1.4, 1.5, 2, 4). Powder X-ray diffraction patterns of the different members synthesized by the method of rapid heating and quenching are shown in Figure 1. Important observations were made on the basis of the special synthetic attempts and the results obtained from the powder X-ray diffraction. Most importantly, Te^{4+} ions are very much essential for the stabilization of the monoclinic columnar rose type bismuth vanadium oxide. Also, the columnar phase is stabilized without the presence of any impurity for a very narrow range of the value of x, $1.30 \leq x \leq 1.40$. Repeated verifications of the bulk syntheses invariably proved the value of x to be 1.35 ± 0.03. Any other amount of Te^{4+} ions, as indicated by the value of x, resulted always in the formation of oxides such as $BiVO_4$

dx.doi.org/10.1021/ic2017159 | Inorg. Chem. 2012, 51, 1462−1470

or $Bi_4V_2O_{11}$, as the case may be (Figure 1). Even the preparation of the bulk stoichiometries for the preferred value of x in the system $Bi_{13-x}Te_xV_5O_{34-\delta}$ ($x = 1.35 \pm 0.03$) was required to be treated under the preheat and quench thermal treatment, since any other alternate thermal treatment involving the slow heating (5−10 °C/min) of the reactants followed by the annealing (5−10 °C/min) led to the formation of small amounts (∼5−10%) of the additional phases such as the $BiVO_4$ or $Bi_4V_2O_{11}$.

The difficulties associated with the bulk synthesis of the oxides $Bi_{13-x}Te_xV_5O_{34-\delta}$ seemed to suggest that oxides such as $BiVO_4$, Bi_2TeO_5, and $Bi_4V_2O_{11}$ were preferred thermodynamically over that of the required bismuth rich columnar type oxide. The successful synthesis of this particular oxide, with a minimum amount of Te^{4+} ($x = 1.35 \pm 0.03$) under the rapid heating and quenching conditions that were employed in the current study, rather suggests the formation of a metastable phase.[37] The synthesis of the crystals belonging to the columnar type structure with an incongruent melting point has been aided by the excess amount of tellurium and vanadium (1:1:1 ratio of Bi_2O_3:TeO_2:V_2O_5), since the crystals of $BiVO_4$ and Bi_2TeO_5 were also present in the melt. The stability of the metastable phase has been found to exist within a temperature range 650−750 °C. Any increase in the temperature would lead to the thermodynamically more stable $Bi_4V_2O_{11}$ oxide and its derivatives. The stringent stoichiometric limitation imposed by the amount of Te^{4+}, along with the critical conditions of preparation, can be justified with the expected oxygen vacancies as we go from $Bi_{12}Te_1Mo_3V_2O_{34}$, $Bi_{11}Te_2Mo_2V_3O_{34}$ to the present $Bi_{11.65}Te_{1.35}V_5O_{34-\delta}$. Furthermore, the lattice parameters and the unit cell volume derived from the powder X-ray diffraction patterns of the different members of the series, $Bi_{13-x}Te_xV_5O_{34-\delta}$ ($x = 1.25, 1.35, 1.4, 1.5, 1.75, 2, 2.5, 4$), did not show any significant variation with the value of x (Figure S3). This information has been particularly useful to infer that the columnar phase obtained has been limited to the stabilization of a single phase with the stoichiometry $Bi_{11.65}Te_{1.35}V_5O_{34-\delta}$.

Having established the minimum amount of Te^{4+} required with respect to the amount of bismuth and vanadium in order to form a columnar rose type structure, we attempted to solve the structure based on the single crystal X-ray diffraction data. The single crystal X-ray diffraction data was collected over a full Ewald's sphere at 180 K. Initially, a crystal was chosen with an indexed lattice parameters $a = 11.4557(5)$ Å, $b = 5.7194(2)$ Å, $c = 11.7684(5)$ Å, and $\beta = 101.209°(4)$ and was assigned an acentric space group ($P2$) based on the systematic absences. The structure was then solved by direct methods and refined using SHELX97[33] incorporated in WINGX suite.[38] The structural model in the acentric space group suffered from many limitations, and a most appropriate solution was obtained in a centrosymmetric space group $P2/c$, based on the data set that was collected using a crystal indexed on lattice parameters, $a = 11.4616(7)$ Å, $b = 5.7131(3)$ Å, $c = 23.5090(18)$ Å, $\beta = 101.071°(6)$ (Table 1). The doubling of the c parameter was confirmed by the comparison of the observed intensities of the $00l$ ($l = 2n$) and $00l$ ($l = 2n + 1$) reflections. We did not omit any reflections during any of the refinement trials. The positions of the heavy bismuth atoms were first located by direct methods and were refined. The vanadium and the oxygen atoms were then located from the difference Fourier map. The difference Fourier did not indicate the presence of any isolated tellurium atom confirming the possibility of tellurium atoms sharing the atomic positions of the bismuth atoms. The

Table 1. Crystallographic Parameters of $Bi_{11.65}Te_{1.35}V_5O_{34-\delta}$

formula	$Bi_{11.65}Te_{1.35}V_5O_{34-\delta}$
cryst syst	monoclinic
space group	$P2/c$ (No. 13)
a [Å]	11.4616(7)
b [Å]	5.7131(3)
c [Å]	23.5090(18)
β [deg]	101.071(6)
V [Å^3]	1510.75(17)
Z	2
molecular wt	3387.21
ρ_{calc} [g/cm^3]	7.439
morphology	triangular
color	light yellow
dimensions (mm^3)	0.14 × 0.08 × 0.05
T [K]	180
wavelength [Mo Kα]Å	0.710 73
monochromator	graphite
scan mode	ω scan
min/max Bragg angle [deg]	2.90/32.62
hkl range	−16 → 16, −8 → 8, −33→33
$F(000)$	2827
μ (mm^{-1})	70.43
R_{int}	0.1032
R_σ	0.0674
abs corr	analytical from crystal shape
refinement	F^2
no. reflns used	4612
no. params	157
$R[F^2 > 2\sigma(F^2)]$	0.0685
wR2	0.1624
GOF (S)	1.090
extinction coeff	0.000 32(3)
$\Delta\rho$/e [Å^{-3}]	7.667/−5.579

structural model in the centric space group ($P2/c$) closely resembled that of the $x = 2$ member of the series $Bi(Bi_{12-x}Te_xO_{14})Mo_{4-x}V_{1+x}O_{20}$. The atomic positions (Table 2) of the bismuth atoms numbering Bi1 to Bi6 forming the infinite columns (Figure 2) seemed to be substituted by Te^{4+} ions. The amount of Te^{4+} ions (1.35 ± 0.03), as determined by the synthesis of the bulk crystalline samples, has been statistically distributed among the Bi1−Bi6 positions. Oxygen atoms numbering O1 to O8 were bonded to these (Bi/Te) positions resulting in a typical $[(Bi/Te)_{12}O_{14}]$ columns (Figure 2). The isolated noncolumnar bismuth preferred to be shifted off the center of inversion because of the presence of the lone pair. One of the vanadium atoms V1 was found to be on the 2-fold axis (2f site); the other vanadium atoms V2 and V3 were found to be in the general (4g) positions. The verification of the anisotropic thermal parameters resulted in a very high value of U_{33} as compared to U_{11} and U_{22} for the V1 vanadium atom, and therefore was forced to split (Table 2) with a V1−V1 distance of 0.656 Å.

One of the oxygen atoms, O10, was found to be unstable, and its position was restrained in the consequent refinement cycles. Usually, the oxygen atoms of the columnar structure type divide themselves into two groups, each with a definite range of thermal parameters. The oxygen atoms (O1−O8) belonging to the column $[Bi_{12}O_{14}]$ have the thermal parameters in the range $0.019 < U_{iso} < 0.03$ Å^2. On the other hand, the oxygen atoms (O9−O18) attached to the metal atoms forming

dx.doi.org/10.1021/ic2017159 | Inorg. Chem. 2012, 51, 1462−1470

Table 2. Positional and Thermal Atomic Parameters for $Bi_{11.65}Te_{1.35}V_5O_{34-\delta}$ (Space Group $P2/c$)

atom	site	SOF	x	y	z	U_{iso}
Bi1/Te1	4*g*	0.89/0.11	0.038 52(7)	0.420 46(15)	0.329 99(3)	0.016 45(19)
Bi2/Te2	4*g*	0.89/0.11	0.161 61(7)	−0.077 18(15)	0.247 37(4)	0.016 22(19)
Bi3/Te3	4*g*	0.89/0.11	0.233 28(9)	−0.009 17(17)	0.408 94(4)	0.0263(2)
Bi4/Te4	4*g*	0.89/0.11	0.361 82(9)	0.483 22(18)	0.321 21(4)	0.0284(2)
Bi5/Te5	4*g*	0.89/0.11	0.275 63(10)	0.4960(2)	0.15463(5)	0.0330(3)
Bi6/Te6	4*g*	0.89/0.11	−0.082 76(11)	0.000 01(19)	0.417 68(5)	0.0352(3)
Bi7	4*g*	0.5	0.491 1(13)	0.525(2)	0.0006(7)	0.0347(12)
V1	4*g*	0.5	0.4895(7)	−0.0022(11)	0.2360(3)	0.0125(16)
V2	4*g*	1.0	0.1703(3)	0.5075(7)	0.48879(14)	0.0173(7)
V3	4*g*	1.0	0.4330(4)	−0.0063(8)	0.0831(2)	0.0318(10)
O1	2*e*	1.0	0.0	0.234(3)	0.25	0.008(3)
O2	2*e*	1.0	0.0	0.724(4)	0.25	0.018(4)
O3	4*g*	1.0	0.2280(13)	0.265(3)	0.3364(6)	0.018(3)
O4	4*g*	1.0	0.2344(14)	0.758(3)	0.3383(7)	0.023(3)
O5	4*g*	1.0	0.2555(17)	0.575(4)	0.2415(8)	0.035(4)
O6	4*g*	1.0	0.1410(14)	0.253(3)	0.6487(7)	0.023(3)
O7	4*g*	1.0	0.1464(14)	0.748(3)	0.6552(7)	0.021(3)
O8	4*g*	1.0	0.0533(14)	0.044(3)	0.3642(7)	0.025(3)
O9	4*g*	1.0	0.383(2)	0.150(4)	0.2613(10)	0.049(5)
O10	4*g*	0.63	0.4853	0.8	0.1984	0.19(10)
O11	4*g*	0.80	0.338(6)	−0.018(13)	0.033(3)	0.17(3)
O12	4*g*	0.90	0.417(6)	−0.026(12)	0.151(3)	0.18(3)
O13	4*g*	1.0	0.516(4)	0.754(8)	0.0771(19)	0.129(15)
O14	4*g*	1.0	0.490(4)	0.241(8)	0.4158(18)	0.127(15)
O15	4*g*	1.0	0.1919(19)	0.458(4)	0.0603(10)	0.045(5)
O16	4*g*	1.0	0.297(2)	0.473(5)	0.4644(11)	0.059(6)
O17	4*g*	1.0	0.1001(17)	0.753(3)	0.4538(8)	0.035(4)
O18	4*g*	1.0	0.091(2)	0.264(4)	0.4678(10)	0.054(6)

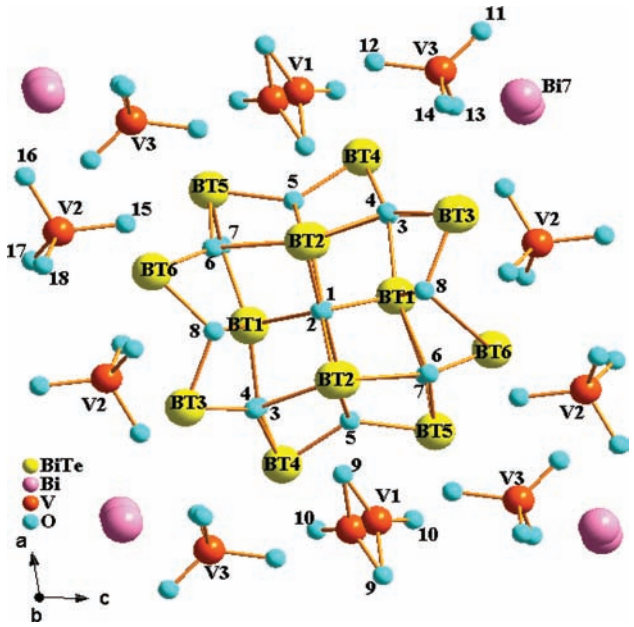

Figure 2. Atomic numbering scheme used for the structural elucidation in the rose type columnar structure of $Bi_{13-x}Te_xV_5O_{34-\delta}$ (BT represents Bi/Te and the oxygen atoms are numbered as 1−18).

the tetrahedral groups such as molybdenum and vanadium tend to have the thermal parameters in the range $0.06 < U_{iso} < 0.18$ Å^2. In the present case, the thermal parameters of the oxygens O10, O11, and O12 attached to V1 and V3 were noted to be even higher than the above-mentioned statistics. The site occupancies were appropriately verified using a constant thermal parameter (U_{iso} = 0.1000), and partial occupancies to an extent of ∼60%, 80%, and 90% were respectively observed for O10, O11, and O12 oxygen atoms. The oxygen content of ∼32.7 resembled closely the expected oxygen count for the stoichiometry $Bi_{11.65}Te_{1.35}V_5O_{32.675}$. Thereby, the oxygen deficiency (δ) has been found to be ∼1.3 for the stoichiometry $Bi_{11.65}Te_{1.35}V_5O_{34-\delta}$, as compared to the oxides without any oxygen deficiencies such as $Bi_{13}Mo_4VO_{34}$, $Bi_{12}Te_1Mo_3V_2O_{34}$, and $Bi_{11}Te_2Mo_2V_3O_{34}$. The final reliability factors based on a model comprising (i) the statistical distribution of Te^{4+} ions in the Bi1−Bi6 positions, (ii) disordered Bi7 and V1 atoms, and finally (iii) the oxygen deficiencies at the O10, O11, and O12 oxygen positions, resulted in R1 = 6.85%, wR2 = 16.24%, S = 1.09 with a difference peak of 7.67 Å^{-3}. The final crystallographic parameters obtained for such a model have been summarized in Table 1. Additionally, the structure has been found to be relieved of the limitations that were noted in the noncentrosymmetric structure (R1 = 7.15%, wR2 = 18.17%, S = 1.233), such as the presence of a high electron density peak ∼16.69 Å^3 in the difference Fourier map (Table S1). The centrosymmetric structure was further justified as shown by the consistent reduction in the standard deviations of the positional and thermal parameters of the various atoms (Table 2) as compared to that of the noncentrosymmetric structure (Table S2).

The basic framework of the structure of $Bi_{11.65}Te_{1.35}V_5O_{34-\delta}$ ($\delta \sim 1.3$) consisting of the infinite $[(Bi,Te)_{12}O_{14}]$ columns with the appropriate oxygen atoms seems robust along the (010) direction without any significant differences in the corresponding (Bi,Te)−O bond distances (Table 3). These columns are surrounded by VO_4 tetrahedra in layers parallel to (100) and

dx.doi.org/10.1021/ic2017159 | Inorg. Chem. 2012, 51, 1462−1470

Table 3. Selected Bond Distances between (Bi/Te)−O and V−O Atoms in Angstroms (Å) (BT Represents Bi/Te)

atoms	distance	atoms	distance	atoms	distance
BT1 O1	2.133(9)	BT4 O4	2.231(16)	Bi7 O16[a]	2.23(3)
BT1 O8	2.292(17)	BT4 O9	2.41(2)	Bi7 O16[a]	2.43(3)
BT1 O3	2.325(15)	BT4 O10	2.6205(10)	V1 O9[a]	1.69(2)
BT1 O7	2.414(16)	BT5 O7	2.037(16)	V1 O9[a]	1.69(2)
BT1 O2	2.532(15)	BT5 O6	2.092(16)	V1 O10[a]	1.43(6)
BT2 O2	2.185(11)	BT5 O5	2.147(19)	V1 O10[a]	1.890(7)
BT2 O5	2.28(2)	BT5 O15	2.25(2)	V2 O15	1.66(2)
BT2 O4	2.340(16)	BT6 O6	2.138(16)	V2 O16	1.67(3)
BT2 O6	2.496(16)	BT6 O8	2.197(17)	V2 O17	1.74(2)
BT2 O1	2.576(13)	BT6 O7	2.248(16)	V2 O18	1.68(3)
BT3 O4	2.130(16)	BT6 O17	2.534(19)	V3 O11	1.45(7)
BT3 O8	2.149(16)	BT6 O18	2.59(2)	V3 O12	1.64(7)
BT3 O3	2.306(15)	Bi7 O13[a]	2.20(5)	V3 O13	1.69(5)
BT3 O17	2.43(2)	Bi7 O13[a]	2.41(5)	V3 O14	1.66(5)
BT4 O3	2.062(15)	Bi7 O14[a]	2.40(5)		
BT4 O5	2.096(19)	Bi7 O14[a]	2.53(5)		

[a]Calculated bond distances for split Bi7 and V1 atoms.

(001) planes, with the isolated Bi atom located in the intersection of these two layers (Figure 3). Also, the oxygen deficiency has been found to be associated especially with the VO_4 tetrahedra. To begin with, out of the three vanadium atoms V1, V2, and V3, only $(V2)O_4$ seemed to have a perfect tetrahedral oxygen surroundings with bond distances ranging from 1.66(2) to 1.74(2) Å (Table 3, Figure 3). The disordered V1 has been found to be bonded to the oxygen atoms O9 and O10, and the distances were 1.69(2)Å for V1−O9 and 1.43(6) and 1.890(7) Å for the V1−O10. Finally, the vanadium oxygen bonding distances widely vary in the case of $(V3)O_4$ tetrahedra and were found to be V3−O11 (1.45(7) Å), V3−O12 (1.64(7) Å), V3−O13 (1.69(5) Å), and V3−O14 (1.66(5) Å). The thermal vibrations have been known to affect the MoO_4 and $(Mo/V)O_4$ tetrahedra in the oxides $Bi_{26}Mo_{10}O_{69}$, $Bi_{13}Mo_4VO_{34}$, $Bi_{12}Te_1Mo_3V_2O_{34}$, and $Bi_{11}Te_2Mo_2V_3O_{34}$, respectively. The average charge of the tetrahedra in the present compound $Bi_{11.65}Te_{1.35}V_5O_{34-\delta}$, in spite of the oxygen deficiencies, seemed to be quite appropriate $[VO_{3.74}]^{2.48-}$ in order to have a higher electrostatic interaction with the $[Bi_{10.65}Te_{1.35}O_{14}]_n^{9.35n+}$ columns.

Apparently the possibility of accommodating the oxygen nonstoichiometry or the oxygen vacancies around the VO_4 tetrahedral units is likely to be feasible only by changing the local coordination of the vanadium atoms. The characteristic Raman bands often provide the local structural information of materials. Figure 4 shows the Raman spectra of

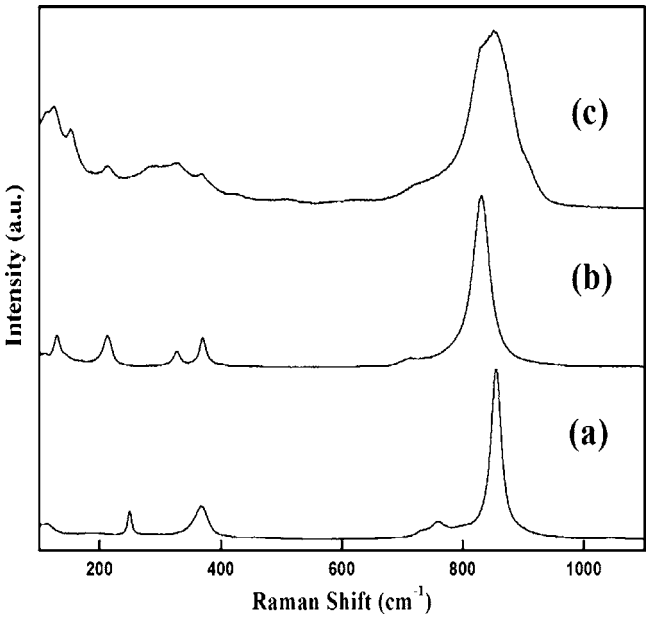

Figure 4. Raman spectra of (a) zircon $BiVO_4$, (b) monoclinic scheelite $BiVO_4$, and (c) $Bi_{11.65}Te_{1.35}V_5O_{34-\delta}$ ($\delta \sim 1.3$).

$Bi_{11.65}Te_{1.35}V_5O_{34-\delta}$ ($\delta \sim 1.3$) in the range 200−1000 cm^{-1}, along with that of the tetragonal ($I4_1/amd$) zircon and monoclinic ($I2/a$) scheelite based $BiVO_4$ as references. The spectra of zircon and scheelite $BiVO_4$ matched well with that of the reported spectra in the literature[39,40] and consist of a very strong symmetric V−O stretching mode around 825−850 cm^{-1}. In addition, the symmetric and the asymmetric deformation modes of VO_4^{3-} have also been observed around 370 and 320 cm^{-1}. In the case of $Bi_{11.65}Te_{1.35}V_5O_{34-\delta}$ ($\delta \sim 1.3$), the presence of VO_4 tetrahedral units is confirmed, and the corresponding V−O stretching mode was observed as a broad band around 800−850 cm^{-1}. Equally important to mention has

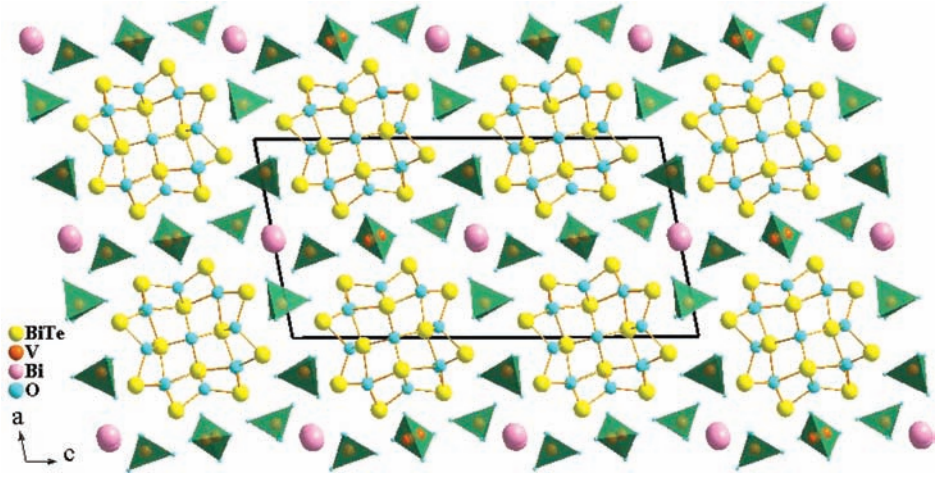

Figure 3. Representation of the rose type columnar structure of $Bi_{11.65}Te_{1.35}V_5O_{34-\delta}$ ($\delta \sim 1.3$) along b projection.

dx.doi.org/10.1021/ic2017159 | Inorg. Chem. 2012, 51, 1462−1470

been the fact that the symmetric and asymmetric deformation modes of VO_4^{3-} are also seen as a very broad band at around 325−370 cm^{-1}. All of the three above-mentioned samples are highly crystalline, and the broadness in the Raman spectra can only be attributed to the change in the oxygen coordination surrounding the vanadium atoms in the $Bi_{11.65}Te_{1.35}V_5O_{34-\delta}$ ($\delta \sim 1.3$) oxide. The presence of the oxygen vacancies in the VO_4 units has been encountered earlier in the zircon based $Ce_{1-x}M_xVO_{4-0.5x}$ (M = Ca, Sr, Pb)[41] and also in the scheelite based $Bi_{1-2x}A_{2x}VO_{4-x}$ (A = Ca, Sr, Cd) oxides.[42] In both the cases, the oxygen vacancies were noted to be disordered as indicated by the absence of a superstructure with a larger cell. In the zircon based oxides, the introduction of oxygen vacancies and the changes in the local coordination around the vanadium atoms have also been substantiated by the appearance similar broad Raman bands.

Finally, we attempted to synthesize the oxides such as $Bi_{12}Te_1V_4MO_{34-\delta}$ (M = Cr, W; $\delta \sim 1$) and $Bi_{11.65}Te_{1.35}V_4MO_{34-\delta}$ (M = Cr, W; $\delta \sim 0.83$), in order to verify independently the columnar phase formation involving V^{5+} ions and to understand the role of Te^{4+} ions in stabilizing the columnar structure. Numerous metal ion (W^{6+}, Cr^{6+}, V^{5+}, P^{5+}, Si^{4+}, Ge^{4+}, Al^{3+}, Mg^{2+}, Li^+) substitutions for Mo^{6+} in the columnar structure have been investigated in the past, and specifically, ions such as Cr^{6+}, W^{6+}, V^{5+} have been preferentially substituted leading to the formation of the solid solution members, $Bi_{26}Mo_{10-x}Cr_xO_{69}$ ($0 \le x \le 5$),[43] $Bi_{26}Mo_{10-x}W_xO_{69}$ ($0 \le x \le 2$),[24] $Bi_{26}Mo_{10-x}V_xO_{69-\delta}$ ($0 \le x \le 4$).[18] Thus, the homogeneous mixtures of the respective starting oxides (Bi_2O_3, TeO_2, V_2O_5, CrO_3, and WO_3) of the compositions such as $Bi_{12}Te_1V_4MO_{34-\delta}$ (M = Cr, W; $\delta \sim 1$) and $Bi_{11.65}Te_{1.35}V_4MO_{34-\delta}$ (M = Cr, W; $\delta \sim 0.83$) were subjected to rapid heating and quenching thermal treatments around temperatures 600, 700, and 750 °C for 12 h. The corresponding powder X-ray diffraction patterns (Figure 5)

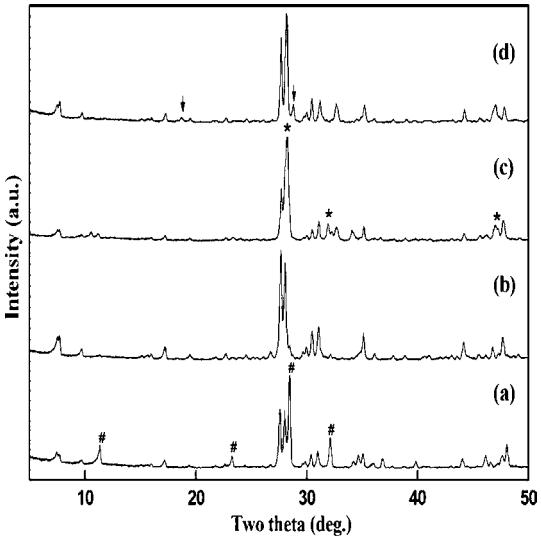

Figure 5. Powder X-ray diffraction patterns of (a) $Bi_{12}Te_1V_4CrO_{34-\delta}$ ($\delta \sim 1$), (b) $Bi_{11.65}Te_{1.35}V_4CrO_{34-\delta}$ ($\delta \sim 0.83$), (c) $Bi_{12}Te_1V_4WO_{34-\delta}$ ($\delta \sim 1$), and (d) $Bi_{11.65}Te_{1.35}V_4WO_{34-\delta}$ ($\delta \sim 0.83$) (#, ↓, and * represent γ-$Bi_4V_2O_{11}$/substituted BIMEVOX (ME = Te), $BiVO_4$, and Bi_2WO_6 phases).

clearly confirmed the columnar phase formation only for the stoichiometries $Bi_{11.65}Te_{1.35}V_4CrO_{34-\delta}$ ($\delta \sim 0.83$) and $Bi_{11.65}Te_{1.35}V_4WO_{34-\delta}$ ($\delta \sim 0.83$). Clearly, the amount of Te^{4+} (1.35) appeared to play a significant role. Additional impurity phases were observed in the case of $Bi_{12}Te_1V_4CrO_{34-\delta}$ ($\delta \sim 1$) and $Bi_{12}Te_1V_4WO_{34-\delta}$ ($\delta \sim 1$). The extent of the substitution of ions such as Cr^{6+}, W^{6+} for V^{5+}, under the influence of the Te^{4+} ions, leading to the formation of the columnar structure, along with their complete structural characterization is currently under investigation.

The UV−vis diffuse reflectance spectra of $Bi_{11.65}Te_{1.35}V_5O_{34-\delta}$ ($\delta \sim 1.3$) and $Bi_{11.65}Te_{1.35}V_4MO_{34-\delta}$ (M = Cr, W; $\delta \sim 0.83$) are shown in Figure 6. The absorption edges for all the three oxides

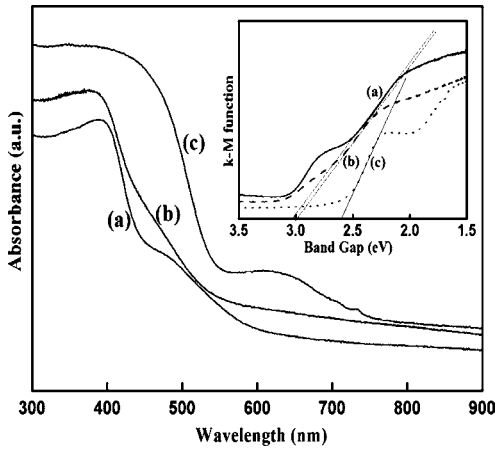

Figure 6. UV−vis absorption spectra of (a) $Bi_{11.65}Te_{1.35}V_5O_{34-\delta}$ ($\delta \sim 1.3$), (b) $Bi_{11.65}Te_{1.35}V_4WO_{34-\delta}$ ($\delta \sim 0.83$), and (c) $Bi_{11.65}Te_{1.35}V_4CrO_{34-\delta}$ ($\delta \sim 0.83$) (inset shows the band gap estimation).

began in the UV region and extended into the visible region. Specifically, the absorption edges have been shifted more toward the visible region by the substitution of Cr^{6+} and W^{6+} ions for V^{5+}. Accordingly, the band gaps were found to be 3.03, 2.98, and 2.60 eV for the oxides $Bi_{11.65}Te_{1.35}V_5O_{34-\delta}$ ($\delta \sim 1.3$), $Bi_{11.65}Te_{1.35}V_4WO_{34-\delta}$ ($\delta \sim 0.83$), and $Bi_{11.65}Te_{1.35}V_4CrO_{34-\delta}$ ($\delta \sim 0.83$), respectively. The valence band of $Bi_{11.65}Te_{1.35}V_5O_{34-\delta}$ may be suggested to be composed of Bi 6s and oxygen 2p orbitals, while V 3d and Te 5s orbitals might contribute to the formation of the conduction band. In the case of other columnar oxides such as $Bi_{11.65}Te_{1.35}V_4MO_{34-\delta}$ (M = Cr, W; $\delta \sim 0.83$), the absorption spectra reflect the contribution of the corresponding chromium 3d or tungsten 5d orbitals. Encouraged by the UV and the extended visible absorption behavior of these columnar oxides, photocatalytic experiments were carried out for the decomposition of organic dyes such as methylene blue (MB) and rhodamine B (Rh B). While noticeable degradation did not happen in the MB solution, the catalysts were found to successfully decompose RhB solution. The photolysis of the dye solution without the presence of the catalysts under the similar experimental conditions has also been included (Figure 7). The experiments revealed moderate rates of decomposition of Rh B under light irradiation, such as 3.409×10^{-3} min^{-1}, 2.98×10^{-3} min^{-1}, and 1.091×10^{-2} min^{-1} for $Bi_{11.65}Te_{1.35}V_5O_{34-\delta}$ ($\delta \sim 1.3$), $Bi_{11.65}Te_{1.35}V_4CrO_{34-\delta}$ ($\delta \sim 0.83$), and $Bi_{11.65}Te_{1.35}V_4WO_{34-\delta}$ ($\delta \sim 0.83$), respectively. While the introduction of Cr^{6+} did not modify the rate of decomposition to a larger extent, the substitution W^{6+} has been found to enhance the photocatalytic activities.

In summary, we have synthesized and characterized a new columnar phase $Bi_{11.65}Te_{1.35}V_5O_{34-\delta}$ ($\delta \sim 1.3$) containing VO_4

dx.doi.org/10.1021/ic2017159 | Inorg. Chem. 2012, 51, 1462−1470

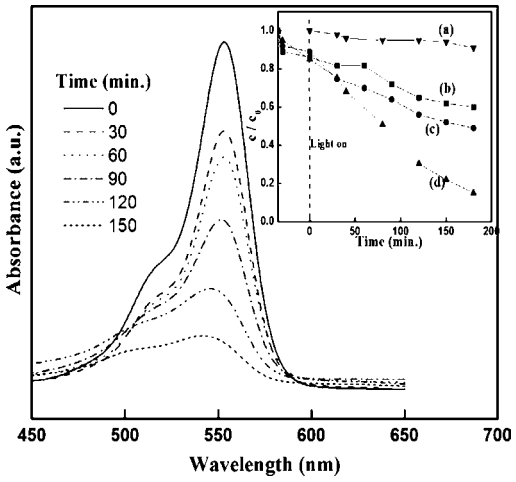

Figure 7. Photocatalytic decomposition of RhB over $Bi_{11.65}Te_{1.35}V_4WO_{34-\delta}$ ($\delta \sim 0.83$) under light irradiation. Inset shows the degradation of RhB (a) without the presence of catalyst, (b) over $Bi_{11.65}Te_{1.35}V_5O_{34-\delta}$ ($\delta \sim 1.3$), (c) over $Bi_{11.65}Te_{1.35}V_4CrO_{34-\delta}$ ($\delta \sim 0.83$), and (d) over $Bi_{11.65}Te_{1.35}V_4WO_{34-\delta}$ ($\delta \sim 0.83$).

tetrahedra, for the first time in the Bi_2O_3–TeO_2–V_2O_5 system. Significantly, Te^{4+} ions are very much essential for the formation of the monoclinic columnar oxide. The stringent stoichiometric limitation imposed by the amount of Te^{4+} ions and the critical conditions of preparation of $Bi_{11.65}Te_{1.35}V_5O_{34-\delta}$ ($\delta \sim 1.3$) suggest the formation of a metastable phase and can be justified by the associated oxygen vacancies. The change in the oxygen stoichiometry caused changes in the local coordination around the V atoms, as revealed by the broad Raman bands in the case of $Bi_{11.65}Te_{1.35}V_5O_{34-\delta}$ ($\delta \sim 1.3$). The higher electrostatic interaction between the $[Bi_{10.65}Te_{1.35}O_{14}]_n^{9.35n+}$ columns and the tetrahedra $[VO_{3.74}]^{2.48-}$ seemed to be quite appropriate for the existence of the present compound. Additional vanadium stabilized columnar structures such as $Bi_{11.65}Te_{1.35}V_4CrO_{34-\delta}$ ($\delta \sim 0.83$) and $Bi_{11.65}Te_{1.35}V_4WO_{34-\delta}$ ($\delta \sim 0.83$) have also been prepared, and the investigation of the photocatalytic efficiencies of these oxides revealed moderate photocatalytic activities for the decomposition of the dyes such as Rhodamine B under UV–vis light irradiation. It will be further interesting to explore the electrical properties of these oxides and the conduction mechanism.

■ ASSOCIATED CONTENT

Ⓢ Supporting Information

Crystallographic information file (CIF) for the single-crystal X-ray refinement. Additional figures and tables. This material is available free of charge via the Internet at http://pubs.acs.org.

■ AUTHOR INFORMATION

Corresponding Author

*E-mail: suma@chemistry.du.ac.in.

■ ACKNOWLEDGMENTS

The authors thank the Department of Science and Technology, Government of India, for the financial support. The authors thank the University Science and Instrumentation Centre (USIC, University of Delhi) especially for the single crystal and powder X-ray diffraction facilities. We thank Dr. R. Nagarajan, Department of Chemistry, University of Delhi, for extending some of the experimental facilities and for constant support. V.T. and N.B. thank UGC and CSIR respectively for their SRF and JRF fellowships.

■ REFERENCES

(1) (a) Zhou, Q.; Kennedy, B. J. *Chem. Mater.* **2003**, *15*, 5025–5028. (b) Chen, Z.; Luo, Z.; Huang, C.; Qi, Y.; Yang, P.; You, L.; Hu, C.; Wu, T.; Wang, J.; Gao, C.; Sritharan, T.; Chen, L. *Adv. Funct. Mater.* **2011**, *21*, 133–138.

(2) Ruiz, P.; Delmon, B. *New Developments in Selective Oxidation by Heterogeneous Catalysis*; Elseviers Science Publishers: New York, 1992.

(3) (a) Boivin, J. C.; Mairesse, G. *Chem. Mater.* **1998**, *10*, 2870–2888. (b) Sahoo, P. P.; Gaudin, E.; Darriet, J.; Guru Row, T. N. *Inorg. Chem.* **2010**, *49*, 5603–5610. (c) Kuang, X.; Li, Y.; Ling, C. D.; Withers, R. L.; Radosavljevic Evans, I. *Chem. Mater.* **2010**, *22*, 4484–4494.

(4) (a) Kudo, A.; Omori, K.; Kato, H. *J. Am. Chem. Soc.* **1999**, *121*, 11459–11467. (b) Tokunaga, S.; Kato, H.; Kudo, A. *Chem. Mater.* **2001**, *13*, 4624–4628. (c) Yu, J.; Kudo, A. *Adv. Funct. Mater.* **2006**, *16*, 2163–2169. (d) Zhou, L.; Wang, W.; Zhang, L.; Xu, H.; Zhu, W. *J. Phys. Chem. C* **2007**, *111*, 13659–13664.

(5) (a) Takahashi, T.; Iwahara, H.; Esaka, T. *J. Electrochem. Soc.* **1977**, *124*, 1563–1569. (b) Harwig, H. A. *Z. Anorg. Allg. Chem.* **1978**, *444*, 151–166. (c) Takahashi, T.; Iwahara, H. *Mater. Res. Bull.* **1978**, *13*, 1447–1453. (d) Punn, R.; Feteira, A. M.; Sinclair, D. C.; Greaves, C. *J. Am. Chem. Soc.* **2006**, *128*, 15386–15387.

(6) (a) Linn, W. J.; Sleight, A. W. *J. Catal.* **1976**, *41*, 134–139. (b) Chen, H.-Y.; Sleight, A. W. *J. Solid State Chem.* **1986**, *63*, 70–75. (c) Pudar, S.; Oxgaard, J.; Chenoweth, K.; Duin, A. C. T.; Goddard, W. A. *J. Phys. Chem. C* **2007**, *111*, 16405–16415.

(7) (a) Egashiraa, M.; Matsuoa, K.; Kagawab, S.; Seiyamac, T. *J. Catal.* **1979**, *58*, 409–418. (b) Antonio, M. R.; Teller, R. G.; Sandstrom, D. R.; Mehicic, M.; Brazdil, J. F. *J. Phys. Chem.* **1988**, *92*, 2939–2944.

(8) (a) Miyazawa, S.; Kawana, A.; Koizumi, H.; Iwasaki, H. *Mater. Res. Bull.* **1974**, *9*, 41–52. (b) Chen, T. U.; Smith, G. S. *J. Solid State Chem.* **1975**, *13*, 288–297.

(9) (a) Abraham, F.; Debreuille-Gresse, M. F.; Mairesse, G.; Nowogrocki, G. *Solid State Ionics* **1988**, *28–30*, 529–532. (b) Abraham, F.; Boivin, J. C.; Mairesse, G.; Nowogrocki, G. *Solid State Ionics* **1990**, *40/41*, 934–937. (c) Kendall, K. R.; Navas, C.; Thomas, J. K.; Loye, H.-C. *Chem. Mater.* **1996**, *8*, 642–649. (d) Patoux, S.; Vannier, R. N.; Mairesse, G.; Nowogrocki, G.; Tarasconn, J.-M. *Chem. Mater.* **2001**, *13*, 500–507. (e) Abrahams, I.; Krok, F. *J. Mater. Chem.* **2002**, *12*, 3351–3362.

(10) (a) Abraham, F.; Ketatni, M. *Eur. J. Solid State Inorg. Chem.* **1995**, *32*, 429–437. (b) Ketatni, M.; Abraham, F.; Mentre, O. *Solid State Sci.* **1999**, *1*, 449–460. (c) Nadir, S.; Swinnea, J. S.; Steinfink, H. *J. Solid State Chem.* **1999**, *148*, 295–301. (d) Giraud, S.; Mizrahi, A.; Drache, M.; Conflant, P.; Wignacourt, J. P.; Steinfink, H. *Solid State Sci.* **2001**, *3*, 593–602. (e) Xun, X.; Yokochi, A.; Sleight, A. W. *J. Solid State Chem.* **2002**, *168*, 224–228. (f) Xun, X.; Uma, S.; Sleight, A. W. *J. Alloys Compd.* **2002**, *338*, 51–53.

(11) (a) Radosavljevic, I.; Evans, J. S. O.; Sleight, A. W. *J. Solid State Chem.* **1998**, *141*, 149–154. (b) Radosavljevic, I.; Evans, J. S. O.; Sleight, A. W. *J. Alloys Compd.* **1999**, *284*, 99–103. (c) Radosavljevic, I.; Sleight, A. W. *J. Solid State Chem.* **2000**, *149*, 143–148. (d) Radosavljevic, I.; Howard, J. A. K.; Sleight, A. W. *Int. J. Inorg. Mater.* **2000**, *2*, 543–550. (e) Ketatni, E. M.; Mernari, B.; Abraham, F.; Mentre, O. *J. Solid State Chem.* **2000**, *153*, 48–54. (f) Xun, X.; Uma, S.; Yokochi, A.; Sleight, A. W. *J. Solid State Chem.* **2002**, *167*, 245–248. (g) Radosavljevic Evans, I.; Tao, S.; Irvine, J. T. S. *J. Solid State Chem.* **2005**, *178*, 2927–2933.

(12) (a) Mizrahi, A.; Wignacourt, J. P.; Steinfink, H. *J. Solid State Chem.* **1997**, *133*, 516–521. (b) Labidi, O.; Wignacourt, J. P.; Roussel, P.; Drache, M.; Conflant, P.; Steinfink, H. *Solid State Sci.* **2004**, *6*, 783–790. (c) Roussel, P.; Labidi, O.; Huve, M.; Drache, M.; Wignacourt, J. P.; Petricek, V. *Acta Crystallogr.* **2009**, *B65*, 416–425.

(13) (a) Sim, L. T.; Lee, C. K.; West, A. R. *J. Mater. Chem.* **2002**, *12*, 17−19. (b) Shimodaira, Y.; Kato, H.; Kobayashi, H.; Kudo, A. *J. Phys. Chem. B* **2006**, *110*, 17790−17797.
(14) (a) Park, J.-H.; Woodward, P. M. *Int. J. Inorg. Mater.* **2000**, *2*, 153−166. (b) Osterloh, F. E. *Chem. Mater.* **2008**, *20*, 35−54.
(15) Kim, H. G.; Hwang, D. W.; Lee, J. S. *J. Am. Chem. Soc.* **2004**, *126*, 8912−8913.
(16) Tang, J.; Zou, Z.; Ye, J. *Angew. Chem., Int. Ed.* **2004**, *43*, 4463−4466.
(17) Thakral, V.; Uma, S. *Mater. Res. Bull.* **2010**, *45*, 1250−1254.
(18) Vannier, R. N.; Mairesse, G.; Abraham, F.; Nowogrocki, G. *J. Solid State Chem.* **1996**, *122*, 394−406.
(19) Buttrey, D. J.; Vogt, T.; Yap, G. P. A.; Rheingold, A. L. *Mater. Res. Bull.* **1997**, *32*, 947−963.
(20) Enjalbert, R.; Hasselmann, G.; Galy, J. *J. Solid State Chem.* **1997**, *131*, 236−245.
(21) Holmes, L.; Peng, L.; Heinmaa, I.; O'Dell, L. A.; Smith, M. E.; Vannier, R. N.; Grey, C. P. *Chem. Mater.* **2008**, *20*, 3638−3648.
(22) Galy, J.; Enjalbert, R.; Rozier, P.; Millet, P. *Solid State Sci.* **2003**, *5*, 165−174.
(23) Enjalbert, R.; Hasselmann, G.; Galy, J. *Acta Crystallogr., Sect. C* **1997**, *53*, 269−272.
(24) Vannier, R. N.; Danze, S.; Nowogrocki, G.; Huve, M.; Mairesse, G. *Solid State Ionics* **2000**, *136*−*137*, 51−59.
(25) Galy, J.; Salles, P.; Rozier, P.; Castro, A. *Solid State Ionics* **2006**, *177*, 2897−2902.
(26) Castro, A.; Enjalbert, R.; Baules, P.; Galy, J. *J. Solid State Chem.* **1998**, *139*, 185−193.
(27) Bastide, B.; Enjalbert, R.; Salles, P.; Galy, J. *Solid State Ionics* **2003**, *158*, 351−358.
(28) Bastide, B.; Villian, S.; Enjalbert, R.; Galy, J. *Solid State Sci.* **2002**, *4*, 599−608.
(29) Begue, P.; Rojo, J. M.; Enjalbert, R.; Galy, J.; Castro, A. *Solid State Ionics* **1998**, *112*, 275−280.
(30) Muktha, B.; Aarthi, T.; Madras, G.; Guru Row, T. N. *J. Phys. Chem. B* **2006**, *110*, 10280−10286.
(31) Vila, E.; Rojo, J. M.; Iglesias, J. E.; Castro, A. *Chem. Mater.* **2004**, *16*, 1732−1739.
(32) Grins, J.; Esmaeilzadeh, S.; Hull, S. *J. Solid State Chem.* **2002**, *163*, 144−150.
(33) SheldrickG. M. *SHELXL97, Program for crystal structure refinement*; University of Gottingen: Germany, 1997.
(34) Brandenburg, K. *DIAMOND (version 3.0), Crystal and Molecular Structure Visualization*; Crystal Impact − K. Brandenburg & H. Putz Gbr: Bonn, Germany, 2004.
(35) Le Bail, A.; Duroy, H.; Fourquet, J. L. *Mater. Res. Bull.* **1998**, *23*, 447−452.
(36) Coelho, A. A. *TOPAS Version 3.1*; Bruker AXS GmbH: Karlsruhe, Germany, 2003.
(37) Gopalakrishnan, J. *Chem. Mater.* **1995**, *7*, 1265−1275.
(38) Farrugia, L. *J. Appl. Crystallogr.* **1999**, *32*, 837−838.
(39) Hardcastle, F. D.; Wachs, I. E.; Eckert, H.; Jefferson, D. A. *J. Solid State Chem.* **1991**, *90*, 194−210.
(40) Yu, J.; Zhang, Y.; Kudo, A. *J. Solid State Chem.* **2009**, *182*, 223−228.
(41) Hirata, T.; Watanabe, A. *J. Solid State Chem.* **2001**, *158*, 254−259.
(42) Uma, S.; Bliesner, R.; Sleight, A. W. *Solid State Sci.* **2002**, *4*, 329−333.
(43) Begue, P.; Rojo, J. M.; Iglesias, J. E.; Castro, A. *J. Solid State Chem.* **2002**, *166*, 7−14.